Journal of
Micro/Nanolithography,
MEMS, and MOEMS

SPIEDigitalLibrary.org/jm3

Investigation of diffraction-based measurement errors in optical testing of aspheric optics with digital micromirror devices

Stephan Stuerwald
Robert Schmitt

Investigation of diffraction-based measurement errors in optical testing of aspheric optics with digital micromirror devices

Stephan Stuerwald[a,*] **and Robert Schmitt**[a,b]
[a]Fraunhofer Institute for Production Technology, Department of Micro and Nanometrology, Steinbachstrasse 17, 52074 Aachen, Germany
[b]RWTH Aachen University, Chair of Metrology and Quality Management, Manfred-Weck-Haus 219, 52074 Aachen, Germany

Abstract. Spatial light modulators (SLMs) have shown to be versatile tools for displays, but also for various applications in optical metrology since light can be individually directed and customized and thus they may serve as flexible masks or holograms. In contrast to SLMs based on liquid crystal on silicon or liquid crystal displays (LCDs), which allow tailoring phase and/or amplitude of a wavefront in transmission or reflection, digital micromirror devices (DMDs) offer highest reflectivity and allow precise as well as fastest guidance of light rays based on the fundamental reflection law. Here, we present and compare different approaches for simulating the diffractive pattern when applying a micromirror device for wavefront readout. The different simulation methods for calculating the diffraction pattern are based on Monte-Carlo simulations in combination with nonsequential ray tracing, on Fourier optics methods (Fourier transform, FT) and on complex digital holographic wavefront propagation. The wavefront measurement concept with the DMDs is based on selecting single subapertures of the wavefront under test and on measuring the wavefront slope consecutively in a scanning procedure. In contrast, in LCD-based approaches already shown in literature, the selection of subapertures and thus the scanning procedure is performed in transmission. The measurement concept and diffraction-based measurement errors of this method will be demonstrated for aspheric optics. Furthermore, different approaches for the prediction and reduction of the diffractive pattern—also based on holographic complex wave front propagation—will be described and characterized. [DOI: 10.1117/1.JMM.13.1.011113]

Keywords: digital micromirror devices; optical testing; hologram; spatial light modulator.

Paper 13126SSP received Jul. 14, 2013; revised manuscript received Dec. 8, 2013; accepted for publication Jan. 10, 2014; published online Feb. 12, 2014.

1 Introduction

Optical, full field testing of aspheres and especially freeform optics still remains a challenging task. Till now, various measurement setups for wavefront characterization have been presented for form and functional testing of aspheres.

The technique with the highest accuracy for optical testing still remains interferometry. However, interferometers are typically expensive and restricted to a lab as they need to be isolated from vibration. Moreover, characterization of aspheres by interferometry typically requires a computer-generated hologram for adaption to the surface of the lens. In general, a spatial light modulator can also serve as a hologram or flexible mask since holograms based on an electron beam manufacturing process are expensive and are specific to each optical element.

To make inline characterization of optics during production, other analysis criteria are used, such as modulation transfer function or, if more information and dynamic range are required, data from a wavefront sensor. A common type of wavefront sensor for those mentioned purposes is Shack–Hartmann, originally developed by German physicist Johannes Hartmann around 1900 and later modified by Roland Shack and Ben Platt in the 1970s. Hartmann's original design consisted of an array of apertures, which was later updated by Shack and Platt by incorporating a lenslet array. The working principle is based on calculating the shift in position of points of light falling through an aperture array compared to where they would fall for a perfect wavefront. The light passing through the lenslets is measured by a CCD sensor [Fig. 1(a)], with a shift in position of the points of light attributed to aberrations in the optic. Wavefront sensors, on the other hand, have advantages as they show why an optic has failed, providing information on the type of aberration. Wavefront sensors can also be used to align and characterize very complex lens objectives, such as those for film cameras or complex lenses for ophthalmology. From the types of aberration, the user can backtrack along an optical path and locate which lens in an objective is faulty.

Systems for functional testing are often based on microlens arrays in front of a photosensitive semiconductor in combination with an analysis logic. Compared to other sensor types for optical testing the Shack–Hartmann sensor (SHS) features a high flexibility with regard to wavefront deformations. In standard, the SHS the measurement capability with regard to the maximum detectable wavefront slope is limited due to the fact that all wavefront subareas are detected simultaneously by an imaging device where the lateral focal areas on the detector must not overlap with neighboring ones in order to avoid ambiguous cases [see Fig. 1(a)]. Thus, the dynamic range is defined by the number of microlenses and the resolution of the imaging sensor. There are several approaches to enhance the dynamic

*Address all correspondence to: Stephan Stuerwald, E-mail: stephan.stuerwald@uni-muenster.de

0091-3286/2014/$25.00

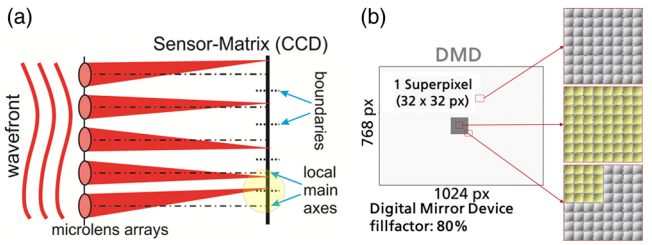

Fig. 1 (a) Conventional principle of Shack-Hartmann–based wavefront sensors, where the lateral distribution of the focal spots of the microlens array is analyzed by a CCD-sensor. Here, overlapping of neighboring sensor fields has to be avoided. (b) Illustration of the mirror matrix of the digital micromirror device (DMD), where every pixel can be controlled in its tilt in the range of [−14, 14] degree. For wavefront scanning, usually subapertures (superpixels) are used to attain higher intensities on the detector which allows faster scanning.

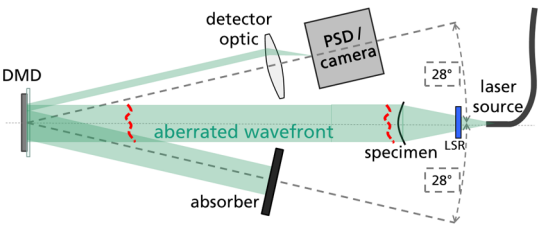

Fig. 2 Schematic drawing of the experimental setup for the lateral wavefront scanning system with enhanced measurable slope range. After transmission of the spherical wavefront, which is adapted to the specimen, the telescope images the approximately collimated, but then aberrated wavefront to the DMD, since the size of ray diameter has to be adjusted and the wavefront has be analyzed directly in the plane after transmission. LSR: light speckle reducer.

range, such as image processing approaches, e.g., spot racking and unwrap algorithms[1]—or the use of additional optical elements, e.g., masks[2,3] or adaptive diffractive microlenses as applied in an adaptive SHS.[4]

In this article, an approach for optical testing is proposed which allows increasing the dynamic range and the lateral resolution at the same time at the expense of the speed one would have if one ran the DMD like a generic Shack–Hartmann array and small aperture effects. The basic idea is to select and thereby encode single subapertures of the wavefront under test and to measure their propagation direction consecutively in a scanning procedure with subapertures [superpixels, Fig. 1(b)]. In difference to the liquid crystal display-based approach described in Ref. 3, here, the selection of the subapertures is performed by a digital micromirror array (DMD). The use of the DMD promises a higher reflectivity or light efficiency, and increased detectable slope range as well as a faster scanning ability (up to several kilohertz). But there are specific challenges as the diffraction effects caused by the small dimensions of the micromirror array and the stability of the signal which will be addressed in this article. The diffraction effects are simulated for different wavelengths and slight changes of the system geometry with regard to tilt. The different simulation approaches are based on the numerical Fourier transform (FT), sequential ray tracing with Monte-Carlo methods as well as complex wavefront propagation. For the complex wavefront propagation, digital holographic techniques are applied, which allow accurate, fast, and complex wavefront propagation. Here, innovative approaches are utilized like the propagation with consideration of the broadband spectrum of low coherent light sources of a supercontinuum light source. For reduction of the diffraction effects and its sidelobes in the diffraction pattern, low-coherent light sources and a speckle reducer (diffuser) are investigated. Furthermore, the calibration of the position sensing device (PSD) is demonstrated in order to ensure highest accuracy and speed despite strong nonlinear effects of the semiconductor elements.

2 Experimental Setup

The experimental setup of the performed investigations is schematically illustrated in Fig. 2. The wavefront to be measured is generated by a point light source—here realized by a fiber-coupled laser diode—which is collimated by the optic under test. The wavefront to be measured is imaged by a telescope in a 4f-arrangement onto a DMD. Afterward, the analysis of the wavefront has significant differences from the SHS. The micromirrors of the DMD can be addressed individually and are used here in two different tilt positions. By means of the DMD and its micromirrors any subaperture can be selected and reflected toward the evaluation unit consisting of detector optic and PSD while the rest of the wavefront is reflected toward an absorber. The analysis is performed by the same principle as for SHS, but with a single asphere to focus the light ray onto the detector, which may be represented by a PSD or a high speed camera. In the back focal plane of the lens the propagation direction of the selected subaperture is transduced into a xy-spot-position, which is detected by position sensor.

The light source is represented by a diode laser and a supercontinuum light source (NKT-Photonics, Danmark, Coheras Super K extreme), which allows a flexible selection of the applied wavelength area via acousto-optical deflectors (AOTF). By this scanning measurement procedure each measurement point can be evaluated with the whole dynamic range of the detector, whereas in conventional SHS the dynamic range of the detector is utilized for evaluation of all measurement subareas in parallel. Thus, the measurement range can be increased without loss of accuracy. Here, a micromirror device (Discovery™ DLp 4100, pixel pitch: 13.68 μm, response time: <20 μm, ~90% fillfactor, Texas Instruments, Texas, Dallas) is applied, which offers more than thousand by thousand mirrors, determining the maximum number of scanned points to one over thousand of the lateral measurement range.

Disadvantageous are the small dimensions of the single micromirrors of the DMD that lead to diffraction effects. The effect of diffraction patterns—caused by the tilted small superpixels for the lateral scan of the wavefront—may lead to errors related to the detected spot centroid on the detector. In order to decrease these effects, a speckle light reducer (LSR 3000, Optotune, Dietikon, Switzerland) is applied, which is based on a dynamic circular oscillation movement of a diffuser membrane or a holographic diffuser. The diffuser is bonded on a polymer membrane that comprises four independent dielectric elastomer actuators, which are controlled in such a way that the diffuser plate is set to a circular movement with a frequency of typically 300 Hz. The frequency of the LSR has to be higher than the

frame rate of the detector, so that the detector performs a temporal integration of the diffraction pattern. The local speckle contrast K is calculated from a reflectance image with the following equation:[5]

$$K = \sigma_S / \langle I \rangle, \tag{1}$$

where σ_S and $\langle I \rangle$ represent the spatial standard deviation and mean pixel intensity in a region of interest, respectively. The speckle contrast thus varies between 0 and 1, 0 representing a homogenous beam without speckles. At a macroscopic level, the speckle ratio depends on the diffusion angle of the LSR and the numerical aperture of the detection system. Here, the reduction factor is: $f = \sqrt{\Theta/\Omega}$, where Θ is the diffusion angle and Ω is the numerical aperture of the detection system.

An integrated, measured wavefront derived from the slope distribution as a direct measurement result of the system is shown in Fig. 3(a) for a plane wavefront. By using a nearly perfectly collimated light beam, the system is calibrated as a first step before the measurement of a specimen, which is usually represented by an aspheric optical element [see Fig. 3(b)]. As frequency of the scanning superpixel, 5 Hz have been applied. The maximum measurable tilt angle of the described preliminary system is ~2- deg deviation of a sphere with a reproducibility of less than 2.5 μrad.

3 Theoretical Basics for Diffraction Simulations

For a precise calculation of the diffraction effects for different wavelengths, which have to be taken into consideration for error estimation and compensation of the central spot detection, the knowledge of the pattern plays a vital role, especially for an optimized data processing and analysis of the diffraction pattern on the detector. Therefore, different approaches have been investigated comprehensively, which comprise the nonsequential ray tracing and the following numerical realizations of the diffraction integral:

- Discrete Fresnel transform (DFT): based on the Fresnel-approximation of the Kirchhoff diffraction integral, one of the main principles of Fourier optics[6]
- Convolution method (CVM) as an alternative numerical realization of the Kirchhoff diffraction integral (see Sec. 3 and Ref. 7)
- Nonsequential ray tracing: Simulation of optical path difference distribution and derived interference pattern.

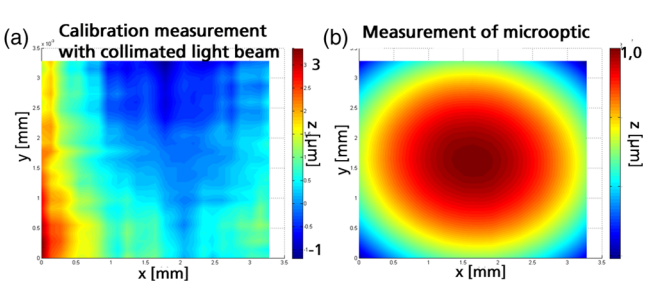

Fig. 3 (a) Calibration measurement of the wavefront scanning system and (b) an exemplarily measurement of an asphere with additional defocus form error.

3.1 *Numerical Propagation of Complex Wavefronts*

The numerical wavefront propagation process of the complex object wave for the purpose of simulating diffraction in a system with a MOEMS-device (here, DMD) can be realized by different numerical methods that calculate the Fresnel–Kirchhoff diffraction integral. Common realizations are the DFT or the CVM.[8,9] The DFT for calculating the wavefront in the plane $(X,\ Y,\ z = d)$ at the distance $z = d$ from the plane at (x_0, y_0, z_0) is usually carried out according to the following (FT) representation, which corresponds to the diffraction integral in Fresnel-approximation:

$$\begin{aligned} O(X,Y,z=d) = {} & \frac{\exp\left(i\frac{2\pi z}{\lambda}\right)}{i\lambda z}\exp\left[i\pi\lambda z\left(\frac{m^2}{N_x^2\Delta x^2}+\frac{n^2}{N_y^2\Delta y^2}\right)\right] \\ & \times\sum_{k=0}^{N_x-1}\sum_{l=0}^{N_y-1} O(x_0,y_0,z_0) \\ & \times\exp\left[i\frac{\pi}{\lambda z}\left(k^2\Delta x^2+l^2\Delta y^2\right)\right] \\ & \cdot\exp\left[-i2\pi\left(\frac{km}{N_x}+\frac{\ln}{N_Y}\right)\right]. \end{aligned} \tag{2}$$

Here, the discrete indices k, l denote the pixels in the hologram plane, m, n those in the reconstruction plane, N the number of pixels in one dimension, and $z = d$ the propagation distance. One disadvantage of these techniques is the simultaneous reconstruction of the reference wave (zero order) and a conjugate complex wave which is known as a twin image of the investigated specimen.[10] The complex object wave $O(x, y, z)$ is propagated from the hologram plane z_0 to the image plane $z = d$.[11]

In general, the reconstruction of the digital hologram in a plane different to the hologram plane can also be achieved using the Fresnel diffraction integral. Let, $O(x_0, y_0, z_0 = 0)$ denote a complex field of an object wave at the object plane $(x_0, y_0, z_0 = 0)$. At a distance of d from an object, the complex field is then given by

$$\begin{aligned} O(X,Y,z=d) = {} & \exp\left(i\frac{2\pi}{\lambda}\frac{X^2-Y^2}{2d}\right) \\ & \times\mathrm{FT}\left[O(x_0,y_0,z_0)\exp\left(i\frac{2\pi}{\lambda}\frac{x_0^2-y_0^2}{2d}\right)\right], \end{aligned} \tag{3}$$

where λ denotes a wavelength. The notation FT denotes an FT operation. Due to the numerically limited size of the applied resolution, the digital hologram has a finite extent. Assuming that the extent is $n \times m$, the digital hologram can be written as

$$O'(X,Y,d) = O(X,Y,d)\mathrm{rect}(X/n)\mathrm{rect}(Y/m). \tag{4}$$

The complex field of the reconstructed object $O(x, y, d)$ can be calculated by[10,12]

$$O(x,y,d) = \exp\left(i\frac{2\pi}{\lambda}\frac{x^2-y^2}{2d}\right) \times \mathrm{FT}\left[O'(X,Y,z_0)\exp\left(i\frac{2\pi}{\lambda}\frac{X^2-Y^2}{2d}\right)\right], = \exp\left(i\frac{2\pi}{\lambda}\frac{x^2-y^2}{2d}\right) \times \mathrm{FT}\left[O(x_0,y_0,z_0)\exp\left(i\frac{2\pi}{\lambda}\frac{x_0^2-y_0^2}{2d}\right)\right] * \mathrm{sinc}\left(\frac{nx}{\lambda d}\right)\mathrm{sinc}\left(\frac{my}{\lambda d}\right), \quad (5)$$

where the notation * denotes a convolution operation. From Eq. (4), the reconstructed object is given by a convolution between the original complex field and a sinc function determined by the extent of the imaging device.

In general, the numerical realization can be performed by utilization of different concepts. As the use of the DFT changes the image diameter in dependence of the propagation distance, convolution-based methods, which preserve the imaging scale, are more applicable in quantitative digital holographic investigations. To achieve a further improvement of the quality of reconstructed, propagated holograms recorded with broad spectral light sources, we propose the following approach in the next section.

3.2 *Reconstruction with Consideration of Spectrum*

If we record digital holograms with light sources like Gaussian shaped spectral functions as an acousto-optical selected part of a supercontinuum light source, which may contain spectral ranges of several tens of nanometers, the complex wave is—in first order—reconstructed and propagated with the central or main wavelength.

Thus, a superposition of complex waves propagated to the image plane with consideration of the normalized spectral distribution $P(\lambda)$ of the light source is proposed. For most light sources with a broad spectral range like LEDs and superluminescence diode (SLDs), but also for AOTF-selected spectra from a continuum light source, a Gaussian spectral distribution can be assumed [Fig. 4(a)], which corresponds to a weighting function in the following calculations:

$$P(\lambda) = \frac{1}{\sqrt{2\pi}\sigma}\exp\left[-\frac{(\lambda-\lambda_c)^2}{2\sigma^2}\right]. \quad (6)$$

If considering the spectral distribution, Eq. (5) has to be extended by an additional integral concerning the wavelength. For a numerical realization, the integral is replaced and approximated by a discrete sum of N complex waves:[13]

$$O'(x,y,d) = \int P(\lambda)\cdot\exp\left(i\frac{2\pi x^2-y^2}{\lambda\ 2d}\right) \times \mathrm{FT}\left[O(x_0,y_0,z_0)\exp\left(i\frac{2\pi x_0^2-y_0^2}{\lambda\ 2d}\right)\right] * \mathrm{sinc}\left(\frac{nx}{\lambda d}\right)\mathrm{sinc}\left(\frac{my}{\lambda d}\right)d\lambda \approx \sum_{j=1}^{N} P'(\lambda_j)\cdot\exp\left(i\frac{2\pi x^2-y^2}{\lambda_j\ 2d}\right) \times \mathrm{FT}\left[O(x_0,y_0,z_0)\exp\left(i\frac{2\pi x_0^2-y_0^2}{\lambda_j\ 2d}\right)\right] * \mathrm{sinc}\left(\frac{nx}{\lambda_j d}\right)\mathrm{sinc}\left(\frac{my}{\lambda_j d}\right), \quad (7)$$

with the discrete normalized spectral distribution $\sum_{j=1}^{N} P'(\lambda_j) = 1$.

The noise, but not the amount of noise in the hologram slightly differs with respect to the chosen wavelength, as the complex field of the diffracted wave depends on the wavelength based on Eq. (4). Here, we assume that the noise is randomly changed in relation to the wavelength. Namely, the intensity of the reconstructed object $I'(x,y,z)$ is assumed to be given by

$$I'_{\lambda_j}(x,y,z) = I_{\lambda_j}(x,y,z) + s_j(x,y,z), \quad (8)$$

where $I_{\lambda j}(x,y,z)$ and $s_j(x,y)$ denote the intensity of the reconstructed object without noise and the noise pattern reconstructed by the wavelength λ_j, respectively. In case of summation of $I'_{\lambda j}(x,y,z)$ over different wavelengths, we have

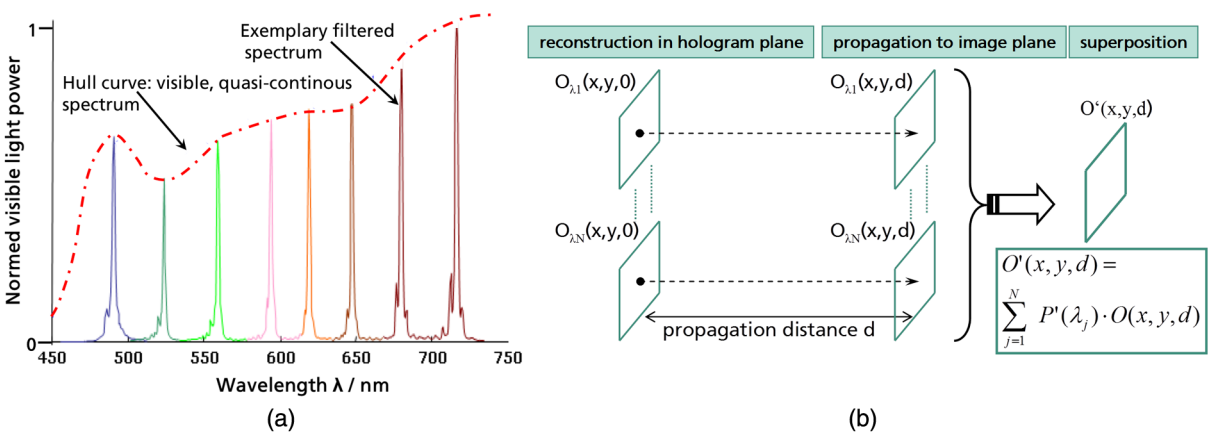

Fig. 4 (a) Spectra of the utilized supercontinuum light source as light sources in the measurement setup. (b) Illustration of the discrete, wavelength selective reconstruction and propagation process with final superposition of waves resulting in $O'(x,y,d)$.

$$\sum_{j=1}^{N} I'_{\lambda_j}(x,y,z) = \sum_{j=1}^{N} P'(\lambda_j)[I_{\lambda_j}(x,y,z) + s_j(x,y,z)],$$

$$\text{with} \sum_{j=1}^{N} P'(\lambda_j) s_j(x,y,z) = S, \tag{9}$$

where the signal noise S is assumed to be constant. As stated above, this equation is based on the assumption of randomly changed noise, which is approximately applicable if the propagation is performed with different wavelengths of a supercontinuum light source. If the constant value S is very small in comparison to $NI'(x,y,z)$, the noise can be neglected in first order, and we obtain the following equation:

$$I'(x,y,z) = I(x,y,z). \tag{10}$$

Therefore, in an analogous way, by superposing the multiple reconstructed complex waves with different wavelengths, the noise is smoothed so that the image quality is improved. The improvement of the reconstruction if using a complex wave addition is compared in Ref. 13 with the addition of the amplitude and phase alone.

4 Results

4.1 *Investigations on Diffraction Effects and Its Compensation for Application of PSD-Detectors*

In Fig. 5(a), a diffraction pattern of a superpixel of 20×20 micromirrors is depicted exemplarily for a laser with a wavelength of 532 nm. The zero and first order can be clearly seen. Especially during scanning operation, one of the first order diffraction patterns may leave the detector surface since the fixed pattern is varying its position in dependence of the wavefront slope. This leads to an error in the analog determination of the center of mass of the intensity and thus to a measurement error of the wavefront slope [see Fig. 5(b)]. Once the pattern for zero degree wavefront slope is centered, the error due to the loss of first order intensity spots can be precalculated for different wavelengths, superpixel sizes and distances with the knowledge of the theoretical intensity pattern. With the help of the sum-signal of the PSD, a missing first order spot on the detector can be detected. In combination with the knowledge of the diffraction pattern, the error of the analog given xy-coordinates of the PSD can be compensated by a preliminary characterized nonlinear response function of the PSD.

In the following, several approaches for calculation of the diffraction pattern have been investigated for a precise prediction and adaption of the error compensating measures in case of application of a PSD as a detector in the experimental setup shown in Fig. 2.

The simulation of the diffraction pattern with the DFT method [Eq. (2)] can be easily realized numerically with a fast Fourier transform in case the reconstruction distance is equal to the source point of the spherical wave, which allows lowest calculation time, especially if approximating a superpixel consisting of 10×10 micromirrors with one mirror surface [see intensity pattern in Fig. 6(a)]. The DFT has been investigated with different wavelengths and tilt angles of the DMD and programmed in a graphical user interface (GUI), without approximating the superpixel [Fig. 6(b)]. In Fig. 6(e), the result of the nonsequential ray tracing is given. The simulated configuration is depicted in Figs. 6(c) and 6(d). Here, the intensity distribution in the detector plane corresponds qualitatively to that of the DFT in Fig. 6(b). Solely, slight differences with regard to the scaling of the distribution occur. In Fig. 6(b), the detector surface is assumed to be several millimeters in diameter and thus, the simulated intensity distribution differs from Fig. 6(e) at a first glance caused by a high resolution and the zoom. In case of smoothing to a lower effective resolution, the pattern becomes more similar to those obtained with the DFT in Fig. 6(e).

The simulations related to the CVM have been performed according to the theory in Sec. 3.1. In general, this approach is especially suitable for detectors in the direct vicinity of the DMD, since the results of this approximation are best for propagation distances, where the quadratic phase factors for a quantized Eq. (5) fulfills the following condition:

$$d \leq \frac{\Delta x^2 N_x}{\lambda}.$$

This means, that above ~10 cm, aliasing is often disturbing the result, which can be improved by padding zeros around the matrix to increase the effective resolution of this operation. For detectors and phase cameras, especially for digital holographic setups, this pattern close to the DMD can be retrieved and a subsequent back propagation can then

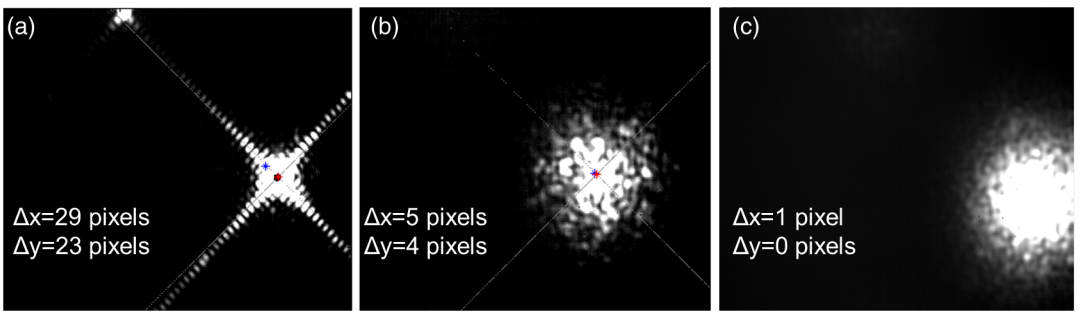

Fig. 5 Recorded diffraction pattern of a DMD-superpixel in the plane of the position sensing device (PSD) at a wavelength of 532 nm with indicated errors in (analog) detected center of mass of intensity distribution: (a) Without speckle reducer (b) with static diffuser plate (c) with active, oscillating speckle reducer.

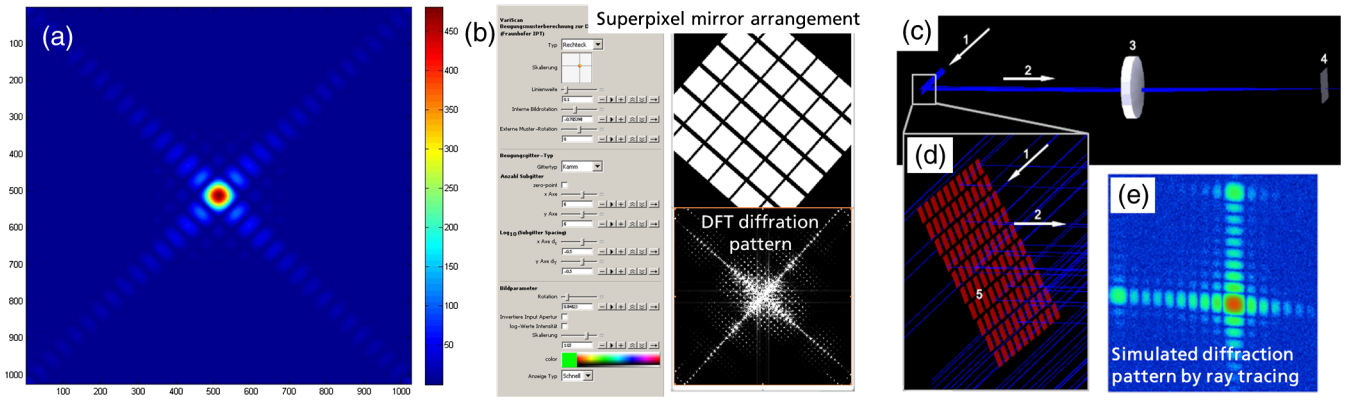

Fig. 6 Simulation of diffraction patterns in detector plane with different numerical approaches: (a) Discrete Fresnel transform (DFT) for a superpixel of 10 × 10 micromirrors approximated as one mirror. (b) The DFT with consideration of limited fillfactor, realized in one multi parameter graphical user interface (GUI). (c) Diffraction based intensity pattern calculated with non sequential ray tracing, therefore based on optical path difference.

reconstruct the original wavefront. With regard to the simulation, some results for the propagation of the complex wavefront of a superpixel within a DMD are shown in Fig. 7. It should be mentioned that the simulation results showed only a negligible effect on the small holes in the center of each micromirror.

In Fig. 7(d), the effect of aliasing can already be observed by the rectangular patterns, which occur with increasing propagation distance. In the near field, each wave of a micromirror can be traced. After several micrometers, the detailed pattern vanishes and a hull distribution rests visible. The transition of those zones and its prediction are helpful in the development process of the measurement system to place a (PSD-) detector at an optimized distance to the DMD.

Experimentally, a speckle reducer consisting of a vibrating diffusor plate has been applied, which causes a statistic averaging during the measurement and light integration time of the sensor [Fig. 8(c)]. The error of the detected center of the diffraction pattern for laser light is shown in Figs. 8(a) and 8(b). It can be seen, that also with modern speckle reducers placed directly in front of the laser fiber, a significant reduction of the diffraction effects and the caused errors can be achieved.

4.2 *Data Acquisition and Processing Strategy*

The data acquisition, processing, and analysis are performed in an integrated GUI (see scheme in Fig. 9). Here, the software is divided into three main blocks, where in the first block the distribution of the tilt states for the whole DMD-matrix is generated for each scan. In a second block, the detector optic is controlled, error compensated according to the calibration measurements and read out. A last data processing block performs a correction of the measured wavefront with regard to the whole system and visualizes the results. The control software allows fast scanning with maximum frequency of the DMD. It is built up modularly and works in parallel threads.

The depicted scheme does not comprise the fundamental system specific calibration routine in order to determine a fixed but usually nonlinear polynomial-based relation between spot center position on the detector and the wavefront slope in x and y direction for each superpixel. This is conducted by calibration samples which have a negligible aberration and highly collimated plane wavefronts. Those wavefronts are varied in their incidence angle in combination with the tilt angle of the DMD-mirrors in order to obtain sufficient calibration data of the system.

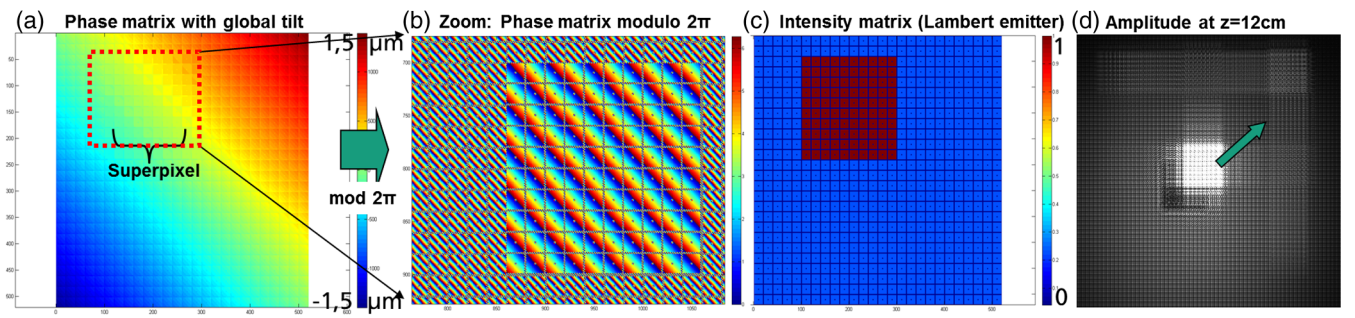

Fig. 7 Simulations and demonstration of building up a complex wave field for calculation of near field intensity distribution of a DMD with a superpixel of 10 × 10 micromirrors: (a) Generated phase mask of a tilted DMD with a superpixel of 10 × 10 pixels. (b) Zoomed phase distribution modulo 2π. (c) Generated intensity distribution. (d) Simulated diffraction pattern by propagation of complex wave front with convolution method (exemplarily for broad band spectrum here).

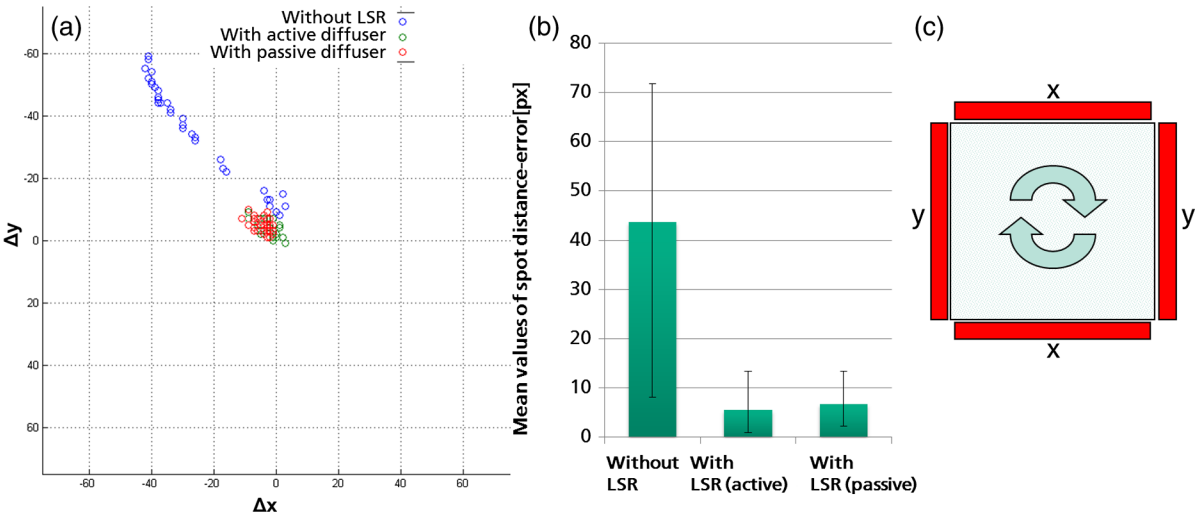

Fig. 8 (a) scatter plot of the PSD-error with regard to its *xy*-output with and without the utilization of the speckle light reducer (unit: pixels). (b) Bar plot of the mean values of spot distance-error in pixels. (c) Illustration of the functionality of a light speckle reducer (LSR, Optotune), which consists of an oscillating diffuser membrane.

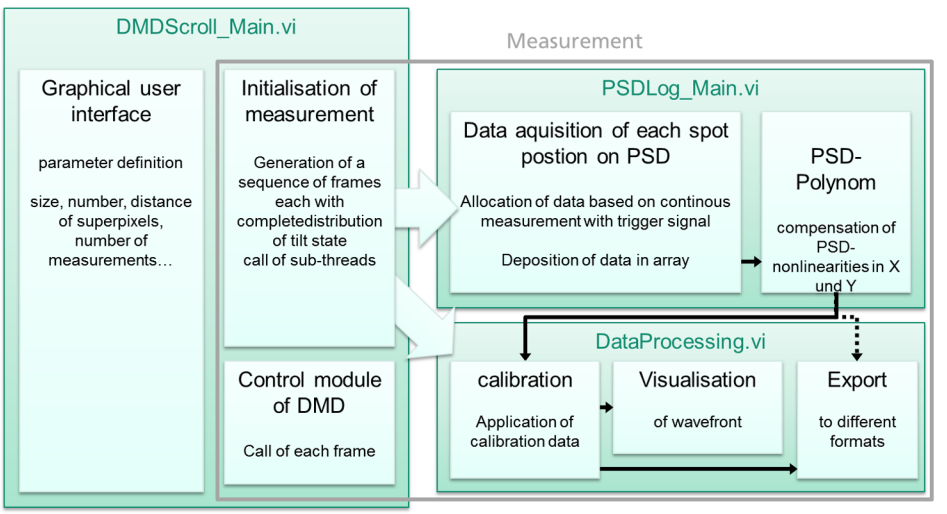

Fig. 9 Schematic illustration of the data acquisition, processing, and analysis implemented in an integrated GUI (based on LabView).

5 Conclusion

The applicability of an innovative setup based on the DMDs for wavefront scanning has been demonstrated with aspheres. Limitations of the configuration are given by the detector module, where the typical diffraction pattern of a DMD with a required superpixel of several micromirrors causes measurement errors when utilizing a PSD due to the limited size of the detector surface. It has been experimentally demonstrated that state of the art speckle light reducers as a compact element can sufficiently reduce the coherence of the light to minimize errors concerning the analog determination of the center of mass of the intensity distribution in the plane of the detector. The investigations show that with the applications of vibrating diffusor plates and holographic diffusor plates, the diffraction effects can be reduced efficiently, which allows the application of low-cost lasers instead of low-coherent light sources like SLDs, which currently do not have enough spectral power to perform measurements for optics lager than typically 3 to 5 cm in diameter. Furthermore, three different theoretical approaches including some simplifications to calculate the effective diffraction patterns have been demonstrated and which correspond with sufficient accuracy to the experimental findings. Future work will mainly address the specific challenges resulting from a feasible, significantly higher measurement range of up to 5-deg deviation from a plane or sphere for a more flexible applicability in inline measurements.

Acknowledgments

This work is funded by the European metrology joint research project EMRP JRP IND10. The application of the theories is based on a project funded by the German Federal Ministry of Education and Research (BMBF).

Furthermore, the support by the participants of the European metrology project with regard to specimens and advice is gratefully acknowledged.

References

1. J. Pfund et al., "Dynamic range expansion of a Shack-Hartmann sensor by use of a modified unwrapping algorithm," *Opt. Lett.* **23**(13), 995–997 (1998).
2. G. Yoon, S. Pantanelli, and L. Nagy, "Large-dynamic-range Shack-Hartmann wavefront sensor for highly aberrated eyes," *J. Biomed. Opt.* **11**(3), 030502 (2006).
3. S. Olivier et al., "Liquid-crystal Hartmann wave front scanner," *Appl. Opt.* **39**(22), 3838–3846 (2000).
4. L. Seifert et al., "The adaptive Shack-Hartmann Sensor," *Opt. Commun.* **216**(4–6), 313–319 (2003).
5. A. Mazhar et al., "Laser speckle imaging in the spatial frequency domain," *Biomed. Opt. Express* **2**(6), 1553–1563 (2011).
6. U. Schnars, "Direct phase determination in hologram interferometry with use of digitally recorded holograms," *J. Opt. Soc. Am. A* **11**(7), 2011–2015 (1994).
7. T. Demetrakopoulos and R. Mittra, "Digital and optical reconstruction of images from suboptical diffraction patterns," *Appl. Opt.* **13**(3), 665–670 (1974).
8. T. Kreis, *Handbook of Holographic Interferometry: Optical and Digital Methods*, Wiley-VCH, Weinheim, Germany (2005).
9. M. Liebling, T. Blu, and M. Unser, "Complex-wave retrieval from a single off-axis hologram," *J. Opt. Soc. Am. A Opt. Image Sci. Vis.* **21**(3), 367–377 (2004).
10. U. Schnars and W. Jüptner, "Direct recording of holograms by a CCD target and numerical reconstruction," *Appl. Opt.* **33**(2), 179–181 (1994).
11. U. Schnars and W. Jüptner, "Digital recording and numerical reconstruction of holograms," *Meas. Sci. Technol.* **13**(9), R85 (2002).
12. A. Weckenmann, J. Hoffmann, and A. Schuler, "Development of a tunnelling current sensor for a long-range nano-positioning device," *Meas. Sci. Technol.* **19**(6), 064002 (2008).
13. S. Stuerwald and R. Schmitt, "Imaging micro-optical components with short coherent digital holographic microscopy," *Proc. SPIE* **7717**, 77170O (2010).

Stephan Stuerwald is a head of the micro and nano metrology group within the Department of Optical Metrology at the Fraunhofer IPT in Aachen. He is also teaching at the RWTH Aachen University. He mainly studied physics and math at the University of Muenster, where he finished his main studies in 2008 and started to be a research fellow at the Fraunhofer Foundation for Applied Research. He finished his works on his first PhD-thesis in 2012.

Robert Schmitt is a head of the Chair of Metrology and Quality Management and member of the board of directors for the Laboratory for Machine Tools and Production Engineering WZL of the RWTH Aachen University. He is also head of the Department of Production Metrology and Quality of the Fraunhofer Institute for Production Technology (IPT) as well as a member of the board of directors of the Fraunhofer IPT.